

# Migration of semiflexible polymers in microcapillary flow

RAGHUNATH CHELAKKOT<sup>1</sup>, ROLAND G. WINKLER<sup>1</sup> and GERHARD GOMPPER<sup>1</sup>

<sup>1</sup> *Institut für Festkörperforschung, Forschungszentrum Jülich, 52425 Jülich, Germany*

PACS 47.61.-k – Micro- and nano-scale flow phenomena

PACS 83.10.Rs – Computational simulations of molecular and particle dynamics

PACS 87.15.-v – Biopolymers: structure and physical properties

**Abstract.** – The non-equilibrium structural and dynamical properties of a semiflexible polymer confined in a cylindrical microchannel and exposed to a Poiseuille flow is studied by mesoscale hydrodynamic simulations. For a polymer with a length half of its persistence length, large variations in orientation and conformations are found as a function of radial distance and flow strength. In particular, the polymer exhibits U-shaped conformations near the channel center. Hydrodynamic interactions lead to strong cross-streamline migration. Outward migration is governed by the polymer orientation and the corresponding anisotropy in its diffusivity. Strong tumbling motion is observed, with a tumbling time which exhibits the same dependence on Peclet number as a polymer in shear flow.

**Introduction.** – The flow properties of soft matter under confinement have been studied intensively in recent years, stimulated by the desire to unravel the behavior of these materials in nano- and microfluidic devices. In such systems, confinement effects, a spatially varying shear rate, and hydrodynamic interactions due to the presence of impenetrable walls, lead to phenomena not observed in bulk systems. Often these three effects are mutually competing, and emergent properties are a result of their combined action.

*Flexible polymers* exhibit interesting conformational, dynamical, and flow properties in the presence of walls and in channels [1–6]. In particular, cross-streamline migration away from the wall has been observed [2, 5–12], which crucially depends on hydrodynamic lift force exerted by the wall [2, 9, 13]. In addition, in channel flow flexible polymers migrate away from the channel center, resulting in a decrease in concentration at the centerline [2, 6, 8]. This originates from the large flow-induced polymer stretching and alignment in the high shear-rate region in the vicinity of a surface, which implies a smaller lateral diffusion than that of the coiled conformations in the channel center. Similarly, migration has been found for *rods* in Poiseuille flow, which has been attributed to their anisotropic mobility (parallel and perpendicular to the rod axis); migration towards the surface has been observed when wall hydrodynamic interactions are neglected [14–16].

*Semiflexible polymers*, such as actin-filaments or short fragments of DNA, are neither rodlike nor are they able to undergo large conformational changes. This poses questions as: What is the influence of hydrodynamics on the polymer distribution? Does stiffness influence migration? How are the conformations affected by the flow? Experiments with actin filaments in microchannels provide evidence for a strong influence of flow on semiflexible polymers [17]; theory and simulations have demonstrated the presence of a hydrodynamic lift force in shear flow [13].

The proper account of hydrodynamic interactions (HI) is essential in simulation studies of fluid flows in channels as is emphasized by the appearance of cross-streamline migration. Recently developed mesoscale simulation techniques, such as Lattice Boltzmann [11, 18], Brownian dynamics with a hydrodynamic tensor [1], and multiparticle-collision dynamics [19, 20], are well suited to study hydrodynamic flows in microchannels and are able to bridge the length- and time-scale gap between the solvent and solute degrees of freedom.

In this letter, we employ multiparticle-collision dynamics (MPC) to study the properties of a confined semiflexible polymer exposed to a microchannel flow. We systematically investigate the influence of the flow rate on the polymer structure, conformations, dynamics, and distribution functions across the channel, and provide new insight into the polymer migration process. Some characteristic polymer conformations in flow are displayed in fig. 1.

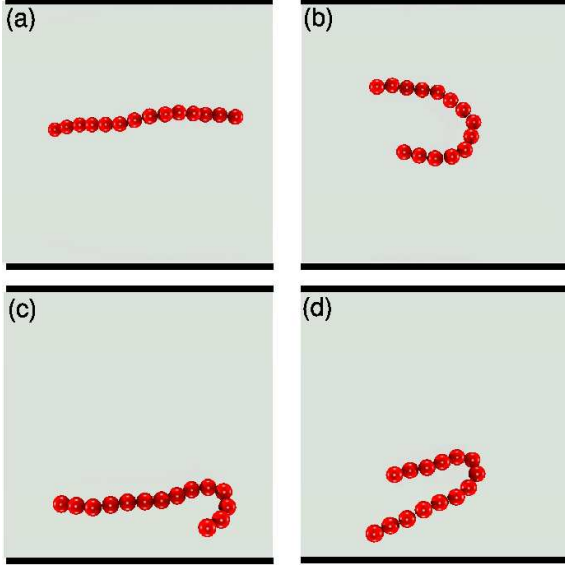


Fig. 1: Polymer conformations for the Peclet number  $Pe = 360$ . (a) Aligned and (b) U-shaped conformations in the center of the channel. (c), (d) Transient hairpin-like conformations outside the center. The flow direction is from left to right. The channel diameter is indicated by the black lines [22].

In addition, we discuss the polymer tumbling dynamics, a property which has been analyzed previously for flexible molecules in both shear and microchannel flows [6, 21].

**Model and simulation method .** — We adopt a hybrid simulation approach to study the properties of semi-flexible polymers in flow, where molecular dynamics simulations (MD) for the polymer are combined with MPC for the solvent [23, 24]. MPC is a particle-based simulation method and proceeds in two steps. In the streaming step, the solvent particles of mass  $m$  move ballistically for a time  $h$ . In the collision step, particles are sorted into the cells of a cubic lattice of lattice constant  $a$  and their relative velocities, with respect to the center-of-mass velocity of each cell, are rotated around a random axis by an angle  $\alpha$  [19, 20, 25]. The fluid is confined in a cylindrical channel with periodic boundary conditions along the channel axis. No-slip boundary conditions are imposed on the channel walls by the bounce-back rule and virtual wall particles [20, 26], and flow is induced by a gravitational force ( $mg$ ) acting on every fluid particle.

The linear polymer is comprised of  $N$  point-like monomers of mass  $M$ , which are connected by linear springs with an equilibrium bond length  $b$ . Excluded-volume interactions are taken into account by the truncated 12 – 6 Lennard-Jones potential, with  $\sigma$  characterizing the bead size and the energy parameter  $\epsilon$  [27]. The bending potential

$$U_b = \frac{\kappa_b}{2} \sum_{i=1}^{N-1} (\mathbf{R}_{i+1} - \mathbf{R}_i)^2 \quad (1)$$

is added to account for stiffness [20], where the  $\mathbf{R}_i$ s are bond vectors and the bending rigidity  $\kappa_b = L_p k_B T / b^3$  is related to the persistence length  $L_p$  for the semiflexible polymer. Since we consider pressure-driven flows, no gravitational force acts on the polymer.

The interaction of a polymer with the solvent is realized by inclusion of its monomers in the MPC collision step [28]. Between two MPC steps, several MD steps are performed to update the positions and velocities of the monomers. Extensive studies of polymer dynamics confirm the validity of this procedure [20, 27–29].

An advantage of the MPC approach is that HI can easily be switched off, without altering the monomer diffusion significantly [30, 31]. In this case, denoted Brownian MPC, each monomer independently performs a stochastic collision with a phantom particle with a momentum taken from the Maxwell-Boltzmann distribution with variance  $m \langle N_c \rangle k_B T$ , where  $\langle N_c \rangle$  is the average number of solvent particles per collision cell [20, 31].

We employ the parameters  $\alpha = 130^\circ$ ,  $h = 0.1\tau$ , with  $\tau = \sqrt{ma^2/k_B T}$  ( $k_B$  is Boltzmann’s constant and  $T$  is temperature),  $\langle N_c \rangle = 10$ ,  $M = m \langle N_c \rangle$ ,  $b = \sigma = a$ , the fluid mass density  $\rho = \langle N_c \rangle m / a^3$ ,  $k_B T / \epsilon = 1$ , and the time step in MD simulation  $h_{MD} = 5 \times 10^{-3} \tau$ . A polymer with  $N = 14$  monomers is placed in a cylindrical channel of radius  $R = 8.5a$ . With the length  $L_r = (N - 1)a = 13a$ , it does not interact with the wall when its center of mass is near the channel center. The persistence length is set to  $L_p = 2Na \approx 2L_r$ . Hence, the polymer shows rod-like behavior at equilibrium. The channel length is  $28a$ . Simulations of the pure solvent system yield velocity profiles which agree with the solution of Stokes’ equation for this geometry. Averages and probability distributions are calculated in the stationary state for various independent initial conditions. To maintain a constant temperature, the velocities are scaled in every collision step and independently in each collision cell [32].

The strength of the applied pressure field is characterized by the Peclet number,  $Pe = \dot{\gamma} \tau_R$ , which is here equal to the Weissenberg number, where  $\dot{\gamma} = g \rho R / (2\eta)$  is the shear rate at the cylinder wall and  $\tau_R$  the polymer relaxation time. The Reynolds number  $Re = \rho R v_m / \eta = \rho R^2 \dot{\gamma} / (2\eta)$ , where  $v_m$  is the maximum fluid velocity, depends linearly on the shear rate. For the above MPC parameters, the viscosity [25] is such that  $Re < 1$  for all considered  $\dot{\gamma}$ . Equilibrium simulations for a system with periodic boundary conditions yield the end-to-end vector relaxation time  $\tau_R \approx 3200\tau$ . This value agrees within approximately 20% with the relaxation time obtained theoretically for a semiflexible polymer with the same ratio  $L_r / L_p$  [21]. The relaxation time of the Brownian MPC simulation is  $\tau_R \approx 8200\tau$ .

**Radial concentration distributions.** — The radial monomer density  $P_{mo}$  is displayed in fig. 2. It is normal-

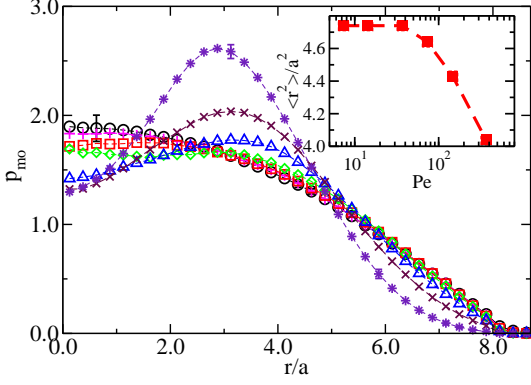


Fig. 2: Radial monomer distributions  $P_{mo}$  for the Peclet numbers  $Pe = 0$  ( $\circ$ ), 7 ( $+$ ), 15 ( $\square$ ), 40 ( $\diamond$ ), 70 ( $\triangle$ ), 150 ( $\times$ ), and 360 ( $\star$ ). Representative error bars are included. Inset: Widths of the distributions as function of the Peclet number.

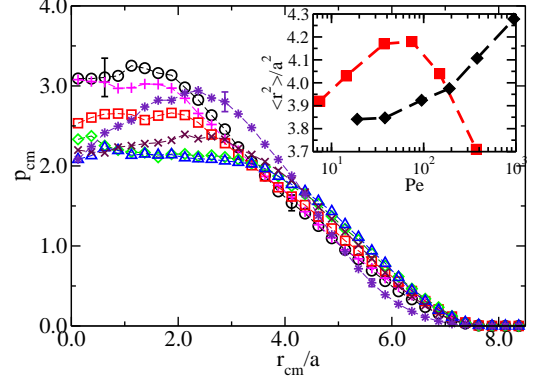


Fig. 3: Radial center-of-mass distribution functions  $P_{cm}$  for the Peclet numbers  $Pe = 0$  ( $\circ$ ), 7 ( $+$ ), 15 ( $\square$ ), 40 ( $\diamond$ ), 70 ( $\triangle$ ), 150 ( $\times$ ), and 360 ( $\star$ ). Inset: Widths of the distributions as function of the Peclet number with (■) and without (◆) HI.

ized such that

$$\int_0^{R/a} r P_{mo}(r/a) dr / a^2 = 1. \quad (2)$$

Without flow, there is a depletion zone close to the channel wall, which extends approximately one radius of gyration into the channel. With increasing Peclet number, the density in the center of the channel decreases, whereas the density near the wall is unchanged. For even larger  $Pe$ , we observe a migration of the molecule away from the surface. At the same time, the density in the channel center decreases further and a maximum develops at a finite distance from the center. The maximum is shifted to smaller radial distances with increasing  $Pe$ . Two effects contribute to the formation of the maximum. On the one hand there is cross-streamline migration of the semiflexible polymer due to hydrodynamic interactions. On the other hand, the flow field causes an alignment of the molecule (see discussion below), which increases the local density at radial positions of strong flow-induced alignment. The width of the distribution function

$$\langle r^2 \rangle = \int_0^{R/a} r^3 P_{mo}(r/a) dr / a^2, \quad (3)$$

shown in the inset of fig. 2, decreases at Peclet numbers  $Pe \gtrsim 50$ , reflecting the inward migration of the polymer.

Figure 3 displays radial center-of-mass distribution functions  $P_{cm}(r_{cm})$  for various Peclet numbers.  $P_{cm}$  displays the same qualitative features as the monomer distribution  $P_{mo}$ , reflecting the same physical mechanism. For  $Pe \lesssim 100$ , the polymer exhibits a migration away from the channel center, which is evident from the decrease of  $P_{cm}$  in the central part of the channel, in qualitative agreement with experiments [17], and its increase near the channel wall. This is supported by the broadening of the width of the distribution with increasing  $Pe$  shown in the inset of fig. 3. For  $Pe > 100$ , the width of the distribution starts

to decrease with increasing  $Pe$ , indicating the presence of a wall-induced lift force. As a consequence, the center-of-mass distribution shows a clear off-centered peak for  $Pe \gtrsim 100$ .

It is interesting to compare these results with those of simulations without HI. We observe an off-center peak in the monomer density distribution (compare fig. 2) also without HI, but the difference between the density in center and at the peak position is smaller. However, the width  $\langle r^2 \rangle$  of  $P_{mo}$  does not decrease with increasing  $Pe$  in the absence of HI. In contrast to the monomer distribution functions, the distinct off-center peak of the center-of-mass distribution (fig. 3) is not present in systems without HI. Here, the width of  $P_{cm}$  increases monotonically with the Peclet number. Hence, without HI, there is an enhanced outward migration due to the lack of the wall-induced lift force. At a first glance, migration without HI seems surprising. However, this is related to the suppression of steric polymer-wall interactions with increasing  $Pe$  due to flow-induced polymer alignment (cf. following section). Hydrodynamic interactions enhance the migration effect, as is seen in fig. 3. Thus, two effects contribute to outward migration: alignment of the semiflexible polymer and intramolecular HI. For the semiflexible polymer, the latter dominates. As discussed in ref. [6], HI are less relevant for strongly confined flexible polymers.

The comparison with confined flexible chains [6] reveals a stronger inward migration for flexible polymers of comparable radius of gyration (and thus larger contour length), as has already been pointed out in ref. [16]. The reason is the stretching of the flexible polymer along the flow direction, which results in a significant longer object than the rodlike molecule and hence a more pronounced migration. Our studies on the stiffness dependence of migration for polymers of equal length show a stronger migration for stiffer molecules.

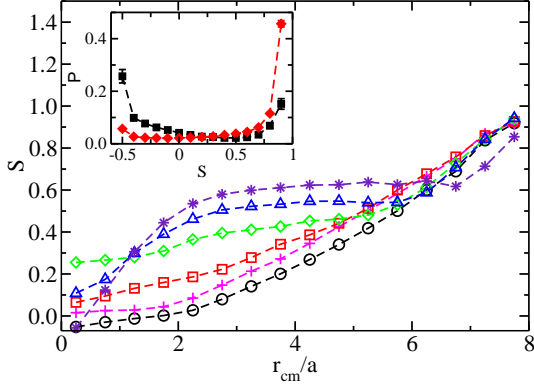


Fig. 4: Orientational order parameters  $S$  as a function of the radial polymer center-of-mass position  $r_{cm}$  for the Peclet numbers  $Pe = 0$  ( $\circ$ ), 7 ( $+$ ), 15 ( $\square$ ), 40 ( $\diamond$ ), 70 ( $\triangle$ ), and 360 ( $\star$ ). Inset: Probability distribution  $P$  of the orientational order  $S = (3\cos^2\theta - 1)/2$  for the Peclet number  $Pe = 360$  and the radial distance  $r_{cm} = 0.5a$  ( $\blacksquare$ ) and  $r_{cm} = 4.5a$  ( $\blacklozenge$ )

**Polymer conformations and alignment.** — In microchannel flow with no-slip boundary conditions, the shear rate varies linearly across the channel. Hence, the force experienced by a polymer depends upon its radial position, and its conformations and alignment are expected to vary as a function of the radial center-of-mass position. Studies of flexible polymers [6] reveal large orientational changes by the imposed flow, which is important for cross-streamline migration [13].

Figure 4 displays the orientational order parameter

$$S(r_{cm}, \theta) = \frac{1}{2} \langle 3 \cos^2 \theta - 1 \rangle, \quad (4)$$

where  $\theta$  is the angle between the polymer end-to-end vector and the flow direction, as a function of its center-of-mass radial position. For  $Pe \lesssim 10$ , the polymer orientation is isotropic in the channel center. For large distances from the center, confinement causes a preferred orientation along the channel axis; the polymer is almost parallel aligned near the channel wall. At  $Pe \gtrsim 50$ , flow induces a strong alignment even at intermediate  $r_{cm}$ . Most importantly, at small radial distances,  $S$  decreases again for  $Pe \gtrsim 100$ , and becomes even negative for very large Peclet numbers, which we attribute to the presence of U-shaped conformations (compare fig. 1a) – as observed experimentally [17]. The probability distributions  $P(S)$  for  $r_{cm} \approx 0.5a$  and  $r_{cm} \approx 4.5a$  reveal the differences in alignment. At small  $r_{cm}$ , the probabilities of U-shaped ( $S = -0.5$ ) and aligned straight ( $S = 1$ ) conformations are much larger than those of all other orientations. In contrast, for larger  $r_{cm}$ , the probability is largest for almost parallel aligned polymers. We like to emphasize that the polymer without HI exhibits very similar orientational order parameters, but only at significantly larger Peclet numbers.

The large probability  $P(S = -0.5)$  (fig. 4) indicates

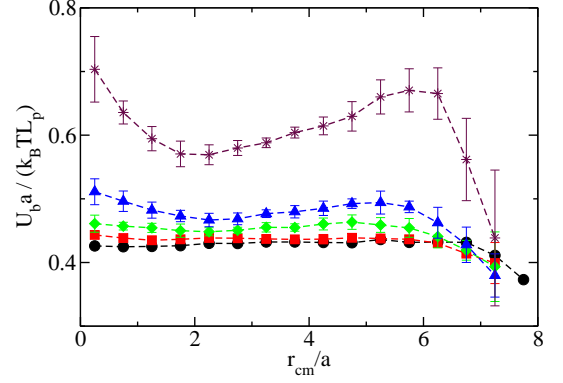


Fig. 5: Scaled polymer bending energies  $U_b$  as a function of radial center-of-mass position for the Peclet numbers  $Pe = 0$  ( $\circ$ ), 15 ( $\blacksquare$ ), 40 ( $\blacklozenge$ ), 70 ( $\blacktriangle$ ), and 360 ( $\star$ ). The increase in bending energy near the center is an indication of U-shaped conformations.

that such conformations are rather stable in the channel center. The snapshot of fig. 1b shows that despite the high bending stiffness the polymer adopts U-shaped conformations. Such conformations can be quantitatively analyzed by calculating the average bending energy  $U_b$ . Figure 5 displays  $U_b$  as function of the radial center-of-mass position and various Peclet numbers. For  $Pe \lesssim 100$  the bending energy is nearly uniform across the channel cross section and decreases near the wall, due to wall induced alignment. Its magnitude is close to the thermal average  $U_b = (L_r/a - 1)k_B T$  of the nearly harmonic bending potential, as expected. An increase in  $Pe$  results in an increase in its absolute value. For  $Pe \gtrsim 100$ ,  $U_b$  is distinctly higher at the channel center due to the formation of a large number of bend conformations. For polymer center-of-mass positions slightly out of the center,  $U_b$  decreases, since the proportion of bend conformations is reduced. With increasing radial center-of-mass position, the local shear rate increases and a polymer assumes transient hairpin conformations, as shown in figs. 1c,d. The average over individual configurations provides a high value for  $U_b$  for such  $r_{cm}$ . Adjacent to the channel wall the bending energy decreases again. Here, the wall interactions lead to a strong alignment with the flow without any bending.

**Lateral displacement.** — The most striking impact of flow on the semiflexible polymer is the strong dependence of its orientation on  $Pe$  and the radial distance. This aspect provides the key to understand the appearance of the off-center maximum in the center-of-mass distribution function.

As is well known, a rod in solution exhibits a larger diffusion coefficient parallel to its axis than perpendicular to it. In the absence of flow, the semiflexible polymer behaves very similar to a stiff rod, we therefore expect that the observed polymer orientational differences across the channel will lead to differences in the lateral dynamic



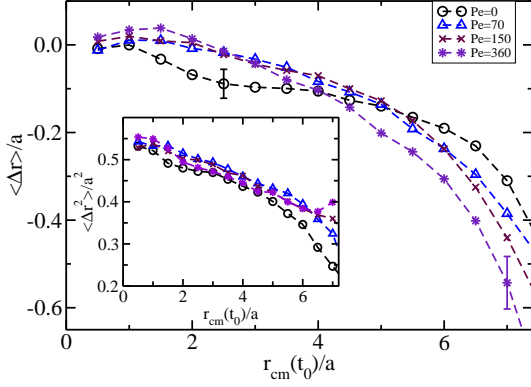


Fig. 6: Mean radial polymer center-of-mass displacements  $\langle \Delta r \rangle = \langle [\mathbf{r}_{cm}(t_0 + \Delta t) - \mathbf{r}_{cm}(t_0)] \mathbf{e}_{cm}(t_0) \rangle$  as function of its radial center-of-mass position  $r_{cm}(t_0)$  for the various indicated Peclet numbers. Inset: Radial polymer center-of-mass mean square displacements  $\langle \Delta r^2 \rangle = \langle (\mathbf{r}_{cm}(t_0 + \Delta t) \mathbf{e}_{cm}(t_0) - \langle \mathbf{r}_{cm}(t_0 + \Delta t) \mathbf{e}_{cm}(t_0) \rangle)^2 \rangle$ .

translational behavior.

In order to characterize this behavior, we present in fig. 6 the radial center-of-mass displacement  $\langle \Delta r \rangle = \langle [\mathbf{r}_{cm}(t_0 + \Delta t) - \mathbf{r}_{cm}(t_0)] \mathbf{e}_{cm}(t_0) \rangle$ ,  $\mathbf{e}_{cm} = \mathbf{r}_{cm}/|\mathbf{r}_{cm}|$ , with respect to the initial radial position  $r_{cm}(t_0)$  of the polymer within a time  $\Delta t$ , which is chosen such that the center-of-mass displacement is less than a monomer size  $a$  and the mean square displacement is linear in time. Figure 6 shows a drift away from the wall for all Peclet numbers and an outward drift for the largest  $Pe$  in the channel center, in agreement with the center-of-mass distribution functions of fig. 3. At  $Pe = 0$ , the drift is governed by steric rod-wall interactions for  $r_{cm} \gtrsim 1.5$ , which is reflected by the decrease of  $\Delta r$  for that range of  $r_{cm}$ . An increase of the flow rate reduces the steric effect by aligning the polymer, however, the wall lift force now leads to an increase of the magnitude of the drift for  $r_{cm}/a \gtrsim 5$ .

The mean square displacement  $\langle \Delta r^2 \rangle = \langle (\mathbf{r}_{cm}(t_0 + \Delta t) \mathbf{e}_{cm}(t_0) - \langle \mathbf{r}_{cm}(t_0 + \Delta t) \mathbf{e}_{cm}(t_0) \rangle)^2 \rangle$ , shown in the inset of fig. 6, displays only a slight dependence on drift for  $r_{cm}/a \lesssim 5$ ; its decrease with increasing  $r_{cm}$  reflects the dependence of the mean square displacement on radial position. Without flow, the polymer orientation is isotropic in the central part of the channel, and it is essentially parallel to the channel axis near the wall. Hence, we see the difference between isotropic and perpendicular diffusive motion originating from intramolecular hydrodynamic interactions. For larger radii, steric wall interactions lead to a decrease of the mean square displacement for low Peclet numbers, whereas lift forces increase  $\langle \Delta r^2 \rangle$  for larger  $Pe$  values.

Non-hydrodynamic simulations yield constant mean square displacements for  $r_{cm}/a \lesssim 5$  for the considered range of Peclet numbers. At larger  $r_{cm}$ , steric wall interactions lead to a decrease of  $\langle \Delta r^2 \rangle$ , similar to that for

$Pe = 0$  in fig. 6.

Hence, we conclude that the center-of-mass distribution function is determined by a competition of the radial outward diffusion of a flow-aligned rod and inward migration caused by a wall-induced lift force [13].

**Polymer tumbling.** — Flexible polymers in shear and Poiseuille flow undergo large conformational changes by tumbling motion, i.e., the polymers exhibit a cyclic stretching and collapse dynamics [21, 33]. Visual examination of the dynamics of the semiflexible polymer also indicates tumbling motion. This cyclic motion is characterized by the tumbling time  $t_T$ . Analytical calculations for a planar shear flow have shown that  $t_T \sim \dot{\gamma}^{-2/3}$  for flexible and rodlike polymers, where  $\dot{\gamma}$  is the shear rate [21]. In order to compute the tumbling time for different  $Pe$ , we determine the cross-correlation function between the mean extensions  $\delta z = z - \langle z \rangle$  and  $\delta r = r - \langle r \rangle$  in flow and radial directions, respectively, which is defined as

$$C_{zr}(t) = \langle \delta z(t_0) \delta r(t_0 + t) \rangle / \sqrt{\langle \delta z^2(t_0) \rangle \langle \delta r^2(t_0) \rangle}. \quad (5)$$

The time dependence of the correlation function is presented in fig. 7. Microchannel flows are more complex in nature compared to planar shear flows. In planar shear flow, the polymer exhibits essentially a two-dimensional behavior, whereas the channel flow is rotational symmetric with respect to the channel axis and more complex conformational transitions appear. Therefore,  $C_{zr}$  is qualitatively different from a similar correlation function in planar shear flow for flexible polymers [33]. In the latter case, at  $Pe > 1$ , the correlation function is asymmetric and displays a minimum and a maximum, whereas we obtain a time-symmetric negative correlation function with a peak at  $t = 0$ . The width of the correlation function decreases with increasing flow strength, which is a measure for the dependence of  $t_T$  on  $Pe$ . Hence, we quantify the tumbling time by the full width at half maximum of  $C_{zr}$  for each value of  $Pe$ . As shown in the inset of fig. 7, the tumbling time decreases as  $t_T \sim Pe^{-0.66}$ , i.e., the exponent is very close to the analytically predicted exponent for planar shear flow [21]. In order to verify the result, a tumbling time is also extracted from the distribution function of the time intervals between consecutive crossings of the end-to-end vector with the plane perpendicular to the flow direction [6]. This distribution decays exponentially ( $\exp(-t/t'_T)$ ) for sufficiently large times. The tumbling time  $t'_T$  exhibits the same dependence on the Peclet number as  $t_T$  obtained from  $C_{zr}$ ; quantitatively it is smaller by approximately a factor 1.5. Hence, both definitions of tumbling time are equivalent for the considered system.

**Summary and Conclusions.** — We have analyzed the flow behavior of an actin-like semiflexible polymer confined in a cylindrical channel. The Poiseuille flow induces a strong radial-dependent polymer alignment parallel to the channel associated with a radially outward migration of its center of mass at low Peclet numbers [14, 15] and

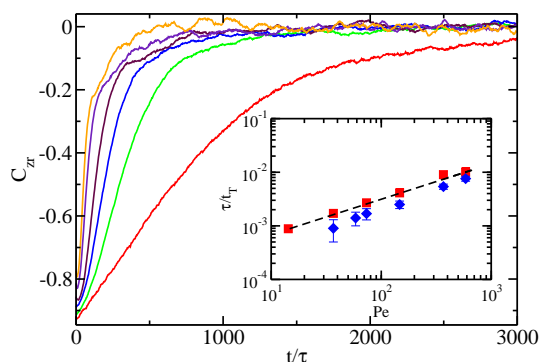


Fig. 7: Cross-correlation functions  $C_{zr}$  for the Peclet numbers  $Pe = 15, 40, 70, 150, 360$ , and  $570$  (bottom to top). Inset: Tumbling times  $t_T$  calculated from the cross-correlation function  $C_{zr}$  (■) and the probability distribution of time intervals between radial orientations of the end-to-end vector (◆).

an inward migration at large  $Pe$ ; both effects are due to hydrodynamic interactions.

This behavior is surprisingly similar to that of a flexible polymer confined in a channel [1, 2, 6, 8–11]. It is caused by the common (flow induced) anisotropy of the polymers, which is responsible for the appearance of migration [13]. Flexible polymers, however, exhibit much more pronounced conformational changes and large deformations, which depend on the radial center-of-mass position, but there is no enhanced probability for U-shaped conformations. We also find different dependencies of the tumbling time on the flow strength [6].

Our studies confirm the importance of HI in microchannel flows. Nevertheless, astonishingly similar distributions and conformations are obtained in simulations without HI, but they appear at significantly larger Peclet numbers. However, in this large  $Pe$  regime, hydrodynamics determines the distributions in the channel. Thus, non-hydrodynamic simulations may provide reasonable structural and conformational properties of a fully hydrodynamic system as long as wall lift forces are negligible, but will fail for large  $Pe$  even qualitatively.

\*\*\*

We thank Thomas Pfohl (Basel) for stimulating discussions. The financial support by the Deutsche Forschungsgemeinschaft within the Priority Program “Nano- and Microfluidics” (SPP 1164) is gratefully acknowledged.

## REFERENCES

- [1] JENDREJACK R. M., DIMALANTA E. T., SCHWARTZ D. C., GRAHAM M. D. and DE PABLO J. J., *Phys. Rev. Lett.* , **91** (2003) 038102.
- [2] JENDREJACK R. M., SCHWARTZ D. C., DE PABLO J. J. and GRAHAM M. D., *J. Chem. Phys.* , **120** (2004) 2513.
- [3] TEGENFELDT J. O., PRINZ C., CAO H., REISNER W. W., RIEHN R., WANG Y. M., COX E. C., STURM J. C., SILBERZAN P. and AUSTIN R. H., *Proc. Natl. Acad. Sci. USA* , **101** (2004) 10979.
- [4] BALDUCCI A., HSIEH C.-C. and DOYLE P. S., *Phys. Rev. Lett.* , **99** (2007) 238102.
- [5] STEIN D., VAN DER HEYDEN F. H. J., KOOPMANS W. J. A. and DEKKER C., *Proc. Natl. Acad. Sci. USA* , **103** (2006) 15853.
- [6] CANNAVACCIUOLO L., WINKLER R. G. and GOMPPER G., *EPL* , **83** (2008) 34007.
- [7] AGARWAL U. S., DUTTA A. and MASHELKAR R. A., *Chem. Eng. Sci.* , **49** (1994) 1693.
- [8] USTA O. B., BUTLER J. E. and LADD A. J. C., *Phys. Fluids* , **18** (2006) 031703.
- [9] MA H. and GRAHAM M. D., *Phys. Fluids* , **17** (2005) 083103.
- [10] KHARE R., GRAHAM M. D. and DE PABLO J. J., *Phys. Rev. Lett.* , **96** (2006) 224505.
- [11] USTA O. B., BUTLER J. E. and LADD A. J. C., *Phys. Rev. Lett.* , **98** (2007) 098301.
- [12] KOHLAE S. C. and KHARE R., *J. Chem. Phys.* , **130** (2009) 104904.
- [13] SENDNER C. and NETZ R. R., *EPL* , **81** (2008) 54006.
- [14] NITSCHKE L. C. and HINCH E. J., *J. Fluid. Mech.* , **332** (1997) 1.
- [15] SCHIEK R. L. and SHAQFEH E. S. G., *J. Fluid. Mech.* , **332** (1997) 23.
- [16] SAINTILLAN D., SHAQFEH E. S. G. and DARVE E., *J. Fluid. Mech.* , **557** (2006) 297.
- [17] STEINHAUSER D. R., *Actin filaments and bundles in flow* (PhD Thesis, University Göttingen, Germany) 2008.
- [18] AHLRICHS P. and DÜNWEG B., *J. Chem. Phys.* , **111** (1999) 8225.
- [19] KAPRAL R., *Adv. Chem. Phys.* , **140** (2008) 89.
- [20] GOMPPER G., IHLE T., KROLL D. M. and WINKLER R. G., *Adv. Polym. Sci.* , **221** (2009) 1.
- [21] WINKLER R. G., *Phys. Rev. Lett.* , **97** (2006) 128301.
- [22] Animations are provided as supplementary material.
- [23] MALEVANETS A. and KAPRAL R., *J. Chem. Phys.* , **110** (1999) 8605.
- [24] IHLE T. and KROLL D. M., *Phys. Rev. E* , **63** (2001) 020201(R).
- [25] RIPOLL M., MUSSAWISADE K., WINKLER R. G. and GOMPPER G., *Europhys. Lett.* , **68** (2004) 106.
- [26] LAMURA A., GOMPPER G., IHLE T. and KROLL D. M., *Europhys. Lett.* , **56** (2001) 319.
- [27] MUSSAWISADE K., RIPOLL M., WINKLER R. G. and GOMPPER G., *J. Chem. Phys.* , **123** (2005) 144905.
- [28] MALEVANETS A. and YEOMANS J. M., *Europhys. Lett.* , **52** (2000) 231.
- [29] WEBSTER M. A. and YEOMANS J. M., *J. Chem. Phys.* , **122** (2005) 164903.
- [30] KIKUCHI N., POOLEY C. M., RYDER J. F. and YEOMANS J. M., *J. Chem. Phys.* , **119** (2003) 6388.
- [31] RIPOLL M., WINKLER R. G. and GOMPPER G., *Eur. Phys. J. E* , **23** (2007) 349.
- [32] HUANG C.-C., CHATTERJI A., SUTMANN G., GOMPPER G. and WINKLER R. G., *J. Comput. Phys.* , **229** (2010) 168.
- [33] TEIXEIRA R. E., BABCOCK H. P., SHAQFEH E. S. G. and CHU S., *Macromolecules* , **38** (2005) 581.